iScience

CellPress
OPEN ACCESS

Article

Catalytic mechanism study of ATP-citrate lyase during citryl-CoA synthesis process

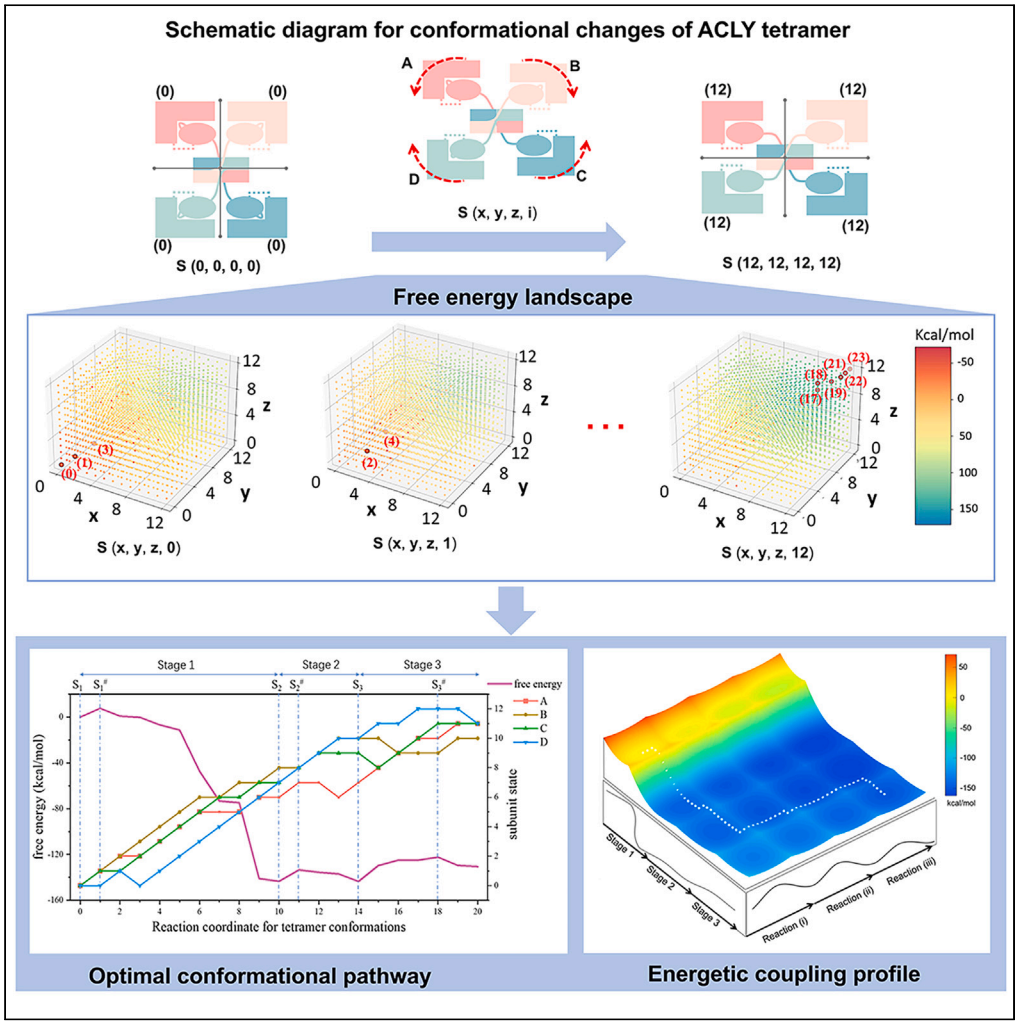

Danfeng Shi, Xiaohong Zhu, Honghui Zhang, Junfang Yan, Chen Bai

baichen@cuhk.edu.cn

Highlights

We constructed free energy landscape of ACLY tetramer with arbitrary symmetries

ACLY tetramer encounters 3 conformational barriers and rigid-D2 symmetry loss

Conformational changes and sub-reactions are energetically coupled for ACLY

Shi et al., iScience 27, 110605
September 20, 2024 © 2024
Published by Elsevier Inc.
https://doi.org/10.1016/j.isci.2024.110605

iScience

CellPress
OPEN ACCESS

Article

Catalytic mechanism study of ATP-citrate lyase during citryl-CoA synthesis process

Danfeng Shi,[1,2,4] Xiaohong Zhu,[1,2] Honghui Zhang,[1] Junfang Yan,[1] and Chen Bai[1,3,5,*]

SUMMARY

ATP-citrate lyase (ACLY) is a critical metabolic enzyme and promising target for drug development. The structure determinations of ACLY have revealed its homotetramer states with various subunit symmetries, but catalytic mechanism of ACLY tetramer and the importance of subunit symmetry have not been clarified. Here, we constructed the free energy landscape of ACLY tetramer with arbitrary subunit symmetries and investigated energetic and conformational coupling of subunits during citryl-CoA synthesis process. The optimal conformational pathway indicates that ACLY tetramer encounters three critical conformational barriers and undergoes a loss of rigid-D2 symmetry to gain an energetic advantage. Energetic coupling of conformational changes and biochemical reactions suggests that these biological events are not independent but rather coupled with each other, showing a comparable energy barrier to the experimental data for the rate-limiting step. These findings could contribute to further research on catalytic mechanism, functional modulation, and inhibitor design of ACLY.

INTRODUCTION

ATP-citrate lyase (ACLY) is a critical central metabolic enzyme, which is highly expressed in the liver, adipose tissue, and cholinergic neurons.[1–3] It utilizes cytoplasmic citrate that generates from the glycolysis process, catalyzing coenzyme A (CoA) to acetyl coenzyme A (Ac-CoA) in an ATP-dependent manner.[4] Ac-CoA then serves as an important bio-synthetic precursor, dominating the synthesis of fatty acids, cholesterol, and acetylcholine.[5] The linkage between the carbohydrate and lipid metabolism makes ACLY a key metabolic checkpoint to sense nutrient availability and coordinate metabolic adaptions.[2,6] It's also suggested that ACLY is required for the increase of histone acetylation in response to growth factor stimulation.[7] The multiple pharmacological effects of ACLY in human body have made it an ideal target for drug development of cardiovascular diseases and cancers.[8,9]

The catalytic cycle of ACLY is reported to be a four-step reaction mechanism with substrate binding, biochemical reactions, and product release happening in a sequential manner.[10–14] The first three steps are accomplished with the stepwise binding of Mg^{2+}-ATP, citrate, CoA, as well as the happening of reactions (i)–(iii) and can be concluded as the citryl-CoA synthesis process (see Figure 1A). Notably, the product of citryl-CoA synthesis process,[15] citryl-CoA,[16,17] also serves as the reactant of the fourth step, namely the citryl-CoA cleavage process.[18] In order to reveal the structural basis for ACLY, recent X-ray crystallographic and cryoelectron microscopy (cryo-EM) studies have demonstrated the basic functional unit of ACLY in its homo-tetramer form, where each subunit consists of an N-terminal citrate synthase (CCS) domain and a C-terminal citrate lyase (CCL) domain.[19–21] According to the biochemical experiments *in vitro*, the binding of different substrates causes variations in the thermal stability and induces conformational oscillations between different states during the citryl-CoA synthesis process.[19] Specifically, upon Mg^{2+}-ATP binding, the His760-located loop (sequence 752–767) could flap between Mg^{2+}-ATP-binding pocket and citrate-binding pocket, mediating the phosphate transfer for reaction (i). The addition of citrate and CoA into the apo state of ACLY tetramer could trigger the swing of the CCS domains around CCL module, resulting in a more compact state relative to the apo form.[21] Crystallographic data indicates that the CCL module also undergoes substantial conformational changes and can adopt open and closed states during the cleavage of citryl-CoA into the reaction products. These findings suggest that substrate binding and the associated reactions are closely linked to substantial conformational changes in both CCS and CCL domains. The binding sites for citrate and CoA are reported to be located in both CCS and CCL domains; however, the potential catalytic function for the binding of citrate and CoA at different domains has not been fully understood. Marmorstein et al. further captured an E599Q-mutant intermediate state of ACLY in complex with CoA and citryl-1-phosphate at the catalytic center of the CCS domain (see Figure 1B), which provide the structural information for the third step of the synthesis process

[1]Warshel Institute for Computational Biology, School of Life and Health Sciences, School of Medicine, The Chinese University of Hong Kong, Shenzhen, Shenzhen 518172, Guangdong, People's Republic of China
[2]School of Chemistry and Materials Science, University of Science and Technology of China, Hefei 230026, China
[3]Chenzhu Biotechnology Co., Ltd, Hangzhou 310005, China
[4]Xuzhou College of Industrial Technology, Xuzhou 221140, China
[5]Lead contact
*Correspondence: baichen@cuhk.edu.cn
https://doi.org/10.1016/j.isci.2024.110605

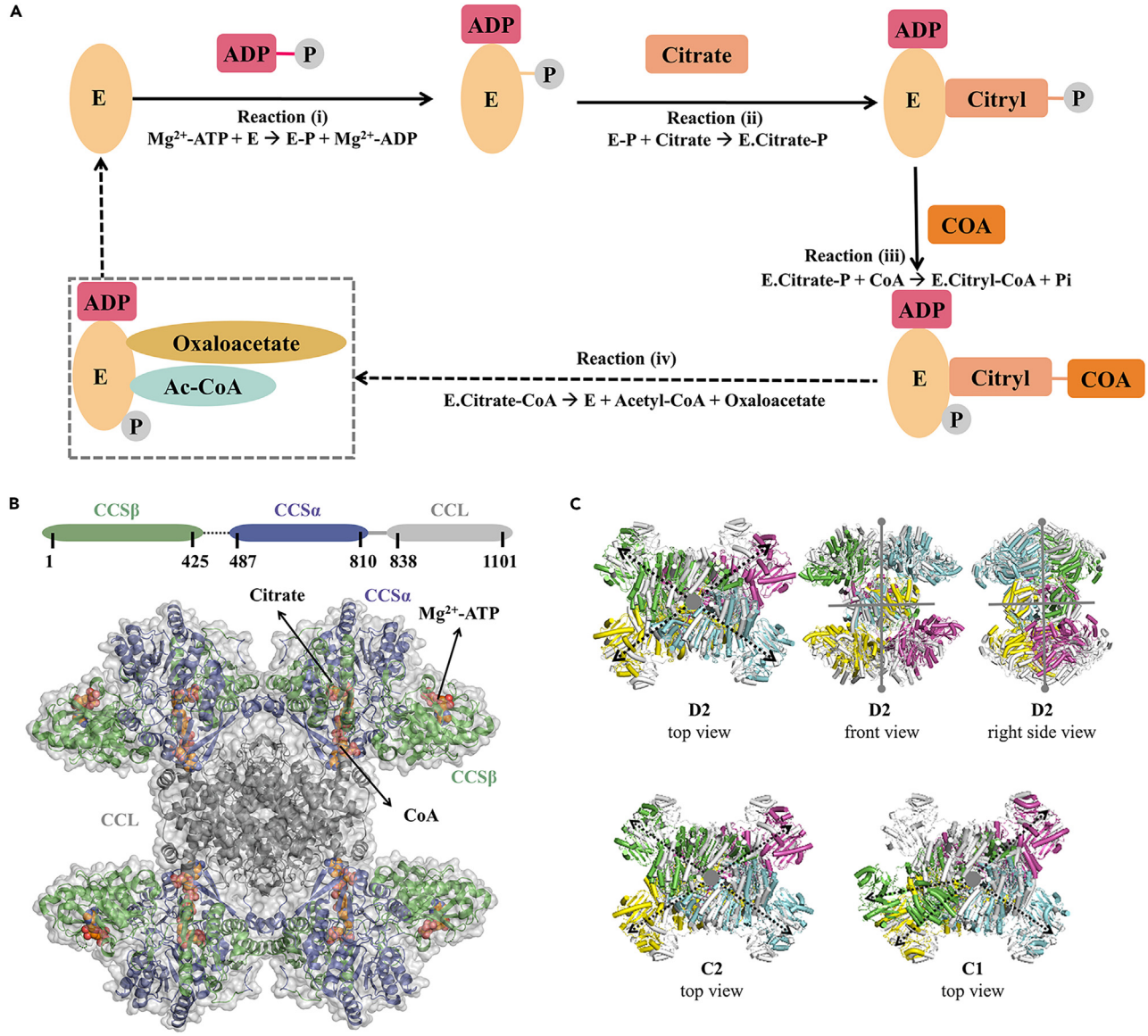

Figure 1. The catalytic cycle, three-dimensional structure and various symmetries of ACLY homo-tetramer

(A) Schematic description of the catalytic cycle of ACLY is divided into the citryl-CoA synthetase reaction process including reaction (i) to reaction (iii) in solid arrow and lytic reaction process including reaction (iv) in dash arrow.

(B) The structural domains and catalytic center of citryl-CoA synthesis for ACLY subunits. CCSβ, CCSα, and CCL domains are shown in green, blue, and gray cartoon respectively. The binding sites of substrates (Mg^{2+}-ATP, citrate, CoA) at the catalytic center of citryl-CoA synthesis are depicted by orange sphere (PDB: 6uuw).

(C) Symmetries of D2, C2, and C1 reported in structural researches for ACLY tetramer. The corresponding three-dimensional structures for D2 symmetry (PDB: 6pof, 6uuw), C2 (PDB: 6qfb), and C1 (PDB: 6uia) are derived from the PDB database and the 2-fold axes for different symmetries are displayed from top, front, and right-side views. The cyro-EM structures of the apo state (E, PDB: 6pof) and the intermediate state (E.Citrate-P.CoA.ADP.Pi, PDB: 6uuw) are applied in the following mechanism research.

toward citryl-CoA.[17,22,23] The detailed conformational and energetic mechanism of ACLY tetramer in the citryl-CoA synthesis process still need to be clarified.

A concerning issue for ACLY is its diverse symmetries for the homo-tetramer form,[24] including C2 and C1 symmetries observed in the crystallographic studies and D2 symmetry modeled in cryo-EM studies (see Figure 1C).[19–21] All reported homo-tetrameric structures of ACLY have CCL domains closely assembling with D2 symmetry at the center of ACLY tetramer while CCS domains stretching outside freely. The CCS or CCL domains from four subunits also engage in close interactions through the mechanism of domain swapping to facilitate functional interconversion between monomers and oligomers in the evolution process.[25] A large number of biological molecular machines assemble as

symmetric homo-oligomers for the favor of stability and finite control of assembly.[26,27] Asynchronous or asymmetric motions have been observed in a symmetric systems to accomplish specific functional goals,[28] as fully symmetric structures are often unfavorable due to considerations of both entropy and interaction enthalpy at the interface of identical subunits.[29] Hence, it is reasonable to consider the symmetric change among different subunits when elucidating the conformational and energetic basis of ACLY tetramer. Furthermore, it is essential to uncover the potential coupling relationship between conformational changes and biochemical reactions during the citryl-CoA synthesis process in order to understand the catalytic mechanism of ACLY.

Modeling large protein systems, such as ACLY tetramer, presents significant challenges due to computational limitations. Currently, obtaining accurate free-energy surfaces through all-atom simulations for biological systems with thousands of residues is extremely challenging. Consequently, researchers have turned to coarse-grained (CG) models to describe these systems.[30–32] Before the CG energy evaluation, the Monte Carlo proton transfer (MCPT) algorithm[31] is applied to control the proton transfer between ionizable residues or between one ionizable residue and the bulk and obtain the charge configuration of the system.[33] The CG model developed by Warshel and coworkers has been demonstrated to be a well-accepted and powerful tool for its better treatment of electrostatics free energy than other CG models[34] and applied to the mechanism research of a series of complex systems, such as F1-ATPase,[35–37] F0-ATPase,[38,39] ribosome,[40,41] and GPCRs.[42,43] It is worth noting that CG models ignore the atomic details for the breaking and formation of chemical bonds when simplifying the representation of amino acid residues in enzyme reaction process. The quantum mechanics (QM) or quantum mechanics/molecular mechanics (QM/MM) approaches for atomic details would be an important supplement to CG models. In this study, we focus on the energy profile of the conformational transitions and aim to the recognition of key residues and energy coupling of different enzymic events,[44] while further QM or QM/MM will be performed in other studies.

In order to reveal the conformational and energetic changes of ACLY tetramer during the citryl-CoA synthesis process, molecular modeling and CG energy evaluation were performed in this study. Starting from two key conformational states of the citryl-CoA synthesis process, a four-dimensional free energy landscape for all possible conformational combination of ACLY subunits was constructed and applied for the exploration of conformational pathway with the optimal free energy barriers. According to the searched optimal conformational pathway, conformations of ACLY tetramer break its rigid D2-symmetric form during the citryl-CoA synthesis process for the energetic advantage to overcome the potential conformational barriers. Further, an energetic coupling analysis between the conformational and biochemical-reaction free energy profiles was further performed, revealing that the conformational changes of ACLY tetramer are partly coupled with the biochemical-reaction events. Additionally, the key residues that significantly affect the conformational free energy barriers have been predicted. The findings of this study could contribute to further research on the catalytic mechanism, functional modulation, and inhibitor design of ACLY.

RESULTS AND DISCUSSION

A four-dimensional free energy landscape is constructed for conformational pathway exploration during the citryl-CoA synthesis process

Currently, two mechanism models exist for the citryl-CoA synthesis process.[22] The model by Marmorstein et al. suggests that CoA first binds to the CCL domain, and then the pantothenyl moiety of CoA translocates to the CCS domain and reacts with CCS-bound citrate and ATP to form citryl-CoA.[21] While the model by Verstraete et al. suggests that CoA binds to the active sites at CCL and CCS domains and reacts with ATP-derived citryl-phosphate to form citryl-CoA, which is further translocated to the CCL domain for cleavage.[19] In both models, the pantothenyl moieties translocate between the CCL and CCS active sites, with the adenosine moieties remaining bound to CoA-binding site of the CCL domain. Despite of the translocation differences between CCS and CCL domains, both mechanism models believe that CoA binds both to the CCL and CCS domains during the citryl-CoA synthesis reaction at the CCS active site. Therefore, we studied the conformational and energetic changes of ACLY during the citryl-CoA synthesis process, and expected to find the optimal possible conformational pathway. A cyro-EM structure at apo state (PDB: 6pof) with no ligand binding and a cyro-EM structure (PDB: 6uuw) at intermediate state with both CoA and citryl-1-phosphate binding to the catalytic center at CCS domain are taken as two key conformations during the citryl-CoA synthesis process and applied for molecular modeling and computation. Both conformational states of ACLY tetramer are determined by imposing D2 symmetry, showing obvious conformational changes at the His760-located loops and CCS domains (see Figure 2A).

In order to enumerate the possible conformational combinations of four subunits in ACLY tetramer, we first explored the conformational pathway of a single subunit by targeted molecular dynamics (TMD). A conformational energy change of $\sim$ -20 kcal/mol is observed between the apo-state and the intermediate-state conformations of a single subunit (see Figure S1A). Thirteen representative subunit states (i.e., subunit 0–12) were selected based on the energy profiles and applied for the construction of tetramer conformations (see Figures S1B and S1C). A total of 13^4 potential tetramer conformations are constructed and each tetramer conformation is depicted as S(x, y, z, i), where x, y, z, and i represent the conformational coordinate for each subunit ranging from 0 to 12. Through further conformational free energy calculation by CG models, the entire free energy landscape for ACLY tetramer conformations were constructed as shown in Figure 2B. An large conformational free energy change of $\sim$ -100 kcal/mol is observed between the apo state S(0, 0, 0, 0) and the intermediate state S(12, 12, 12, 12), indicating that the conformational transition for the citryl-CoA synthesis process tend to exhibit significantly higher conformational stability compared to the apo state. Subsequently, a pathway search procedure was performed to search the optimal conformational pathway with the best energy barriers from S(0, 0, 0, 0) to S(12, 12, 12, 12).

The detailed workflow chart of the procedure was integrated by rescaling of the original free energy landscape, sampling of possible conformational pathways, and scoring of sampled pathways to obtain the optimal conformational pathway (see Figure S2). In order to collect

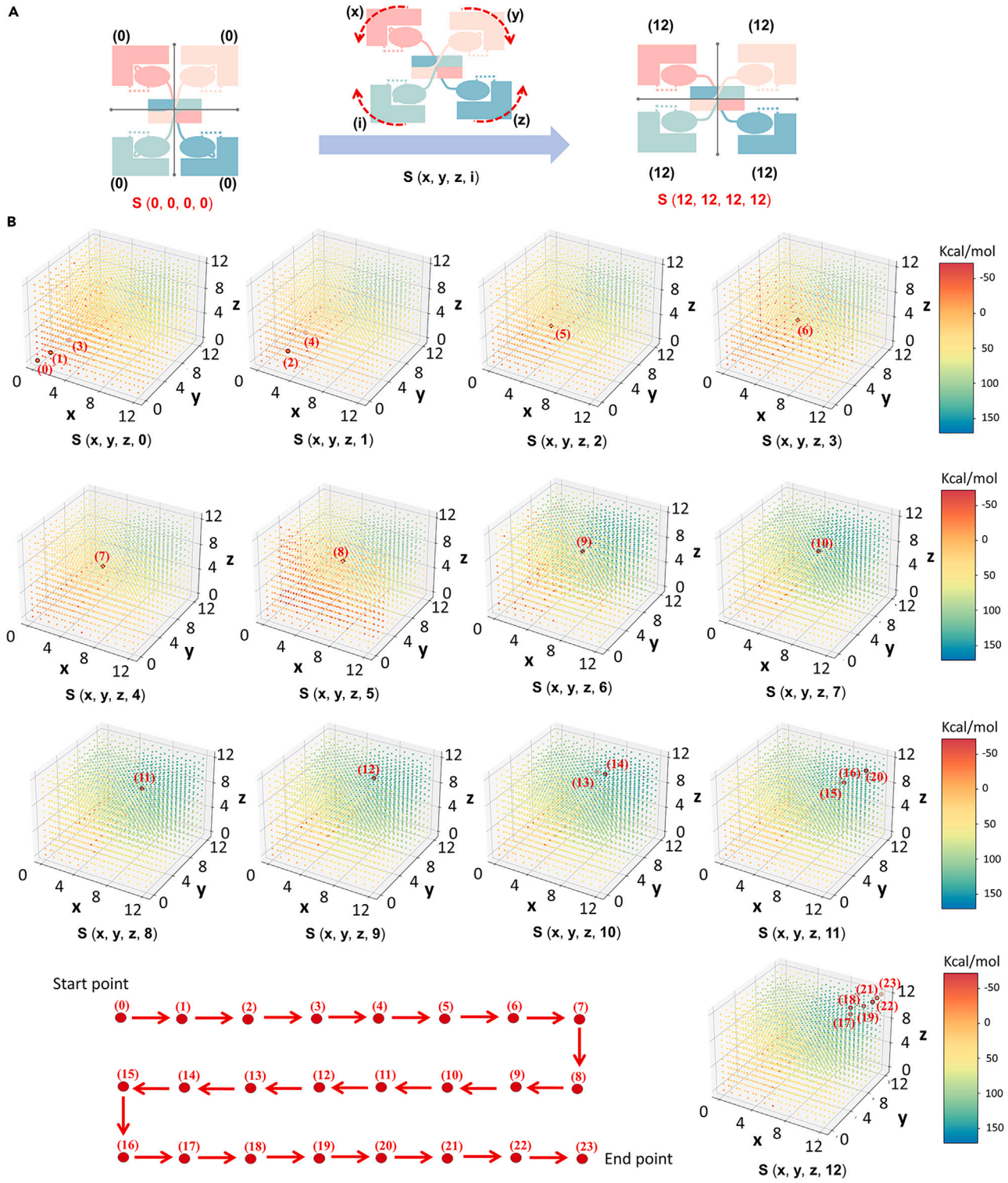

Figure 2. The entire free energy landscape for ACLY tetramer with arbitrary symmetry in citryl-CoA synthesis process

(A) A schematic diagram illustrates the conformational change process of ACLY tetramer, transitioning from S(0, 0, 0, 0) to S(12, 12, 12, 12). The x, y, z, i axes represent the conformational coordinates of four subunits and all possible intermediate conformations of ACLY tetramer are denoted as S (x, y, z, i).

Figure 2. *Continued*

(B) A total of 13^4 conformational states are utilized to construct the entire free energy landscape for ACLY tetramer during the citryl-CoA synthesis process. These states are displayed through 13 cubic boxes. The conformational degrees of freedoms (DOFs) of monomers A, B, and C are represented by (x, y, z) coordinates in each cube, while the conformational DOF of the fourth monomer is represented by the change in the number of cubes ranging from 0 to 12. The color bar indicates the free energy values changing from −160 kcal/mol to 80 kcal/mol. The optimal conformational pathway for ACLY tetramer is marked with red dots in each cubic box and sequentially numbered by Arabic numbers. The moves between red dots are shown by red arrow.

the conformational pathway with best energetic barriers, we introduced a perturbation factor during the conformational sampling. Specifically, each monomer subunit has a certain probability of undergoing conformational changes in the reverse direction (i.e., conformational reverse coefficient, P_{-1}). We conducted Monte Carlo sampling process with different reverse coefficients on the rescaled free energy landscape. It is observed that as the reverse coefficient increases from 0.1 to 0.3, the numbers of moving steps and encountered energy barriers in the sampling pathway also increase, as a result, the overall score of the sampling pathway tends to be lower (see Figure S3). By comparing the energetic profiles for the optimal pathways under various reverse coefficients (see Figure S4), we observe that the decreasing trend of conformational free energies becomes more moderate with a higher value of the reverse coefficient; nevertheless, the sampled optimal pathways all exhibit four energy barriers. As a final choice, we opted a reverse coefficient of 0.1 for further analysis of sampled conformational pathways. The optimal energetic and conformational pathway were further projected into the free energy landscape (see Figure 2B and Video S1), which shows a 23-step flip between S(0, 0, 0, 0) and S(12, 12, 12, 12).

The initial D2 symmetry of ACLY tetramer is broken for the benefit of energetic advantage

As shown in Figure S5, a significant free energy barrier of ∼30 kcal/mol is observed in the final steps of the 23-step conformational pathway, suggesting that the intermediate conformation of S(11, 10, 11, 11) is more energetically favorable than the cyro-EM structure of S(12, 12, 12, 12). We then compared the conformational and energetic differences between subunit 11 and subunit 12. During the conformational transition pathway for a single subunit, the subunit 11 shows a more stable conformational energy than subunit 12, and the change in interaction between E599 and H760 accounts for the main shift in conformational energies (see Figure S6). As the conformational state of S(12, 12, 12, 12) is proposed to be defective in the citryl-CoA synthesis process,[21] its E599Q mutation might possibly alter the subunit states in the wild-type ACLY. The binding modes of citrate and CoA interacting with subunit 10, 11, and 12 were further constructed and compared to the cyro-EM structure of S(12, 12, 12, 12) as shown in Figure S11. It can be seen that binding poses for CoA and citrate are gradually approaching the locations of intermediate ligands in the cyro-EM structure, showing that subunit 11 are ready for the ligand binding of citrate and CoA with better binding free energy than subunit 12 (Table S1). Therefore, S(11, 10, 11, 11) is taken as an important intermediate conformation of the citryl-CoA synthesis process in close proximity to S(12, 12, 12, 12), and the entire conformational change of ACLY tetramer is tracked in 20 steps.

The entire conformational free energy profile exhibits an overall energy-decreasing process, which is divided into three stages according to the occurrence of significant free energy barriers. As shown in Figure 3A, stage 1 represents the process from S_1(0, 0, 0, 0) to S_2(6, 8, 7, 7) with a substantial free energy change of −143.37 kcal/mol, and the key transition state occur at $S_1^{\ddagger}$(1,1,1,0) with a low free energy barrier of 7.56 kcal/mol. It is suggested that the apo state of ACLY tetramer is located at relatively high-energetic level and could be easily activated under the extra energy supply, subsequently reaching a more energy-favorable state quickly and spontaneously. Compared to stage 1, stage 2, and stage 3 are both situated at relatively low-energetic states, showing free energy changes of −0.12 kcal/mol and 12.99 kcal/mol, free energy barriers of 9.98 kcal/mol and 21.16 kcal/mol respectively. The subunit states and symmetries along the conformational pathway are further analyzed, as shown in Figure 3B. No hypothetical D2-symmetic tetramer conformations are observed in sampled intermediate conformations along the pathway. The root-mean-square deviation (RMSD) between sampled intermediate conformations and hypothetical D2-symmetirc conformations (see Figure S7A) shows that sampled intermediate conformations have minor deviations comparing to the nearest hypothetical D2-symmetirc conformation. Moreover, the sampled conformational pathway exhibits lower free energy barrier than the hypothetical D2-symmetric conformational pathway with approximate energetic profiles (see Figure S7B). It suggests that four subunits of the tetramer conformation may not maintain strict D2 symmetry but exhibit diverse subunit states for the purpose of gaining energetic advantages.

Currently, the functional unit of homo tetramer has revealed the structural basis for the cooperation between four ACLY subunits, but how this cooperation happens during the citryl-CoA synthesis process is still unclear. On one hand, citryl-CoA synthesis may occur as a concerted or coordinated process between the different CCS modules; On the other hand, the ciryl-CoA synthesis process in the different CCS modules could occur independently. Here, the citryl-CoA synthesis process is reflected by the conformational change of ACLY subunit, and the symmetry analysis of subunit states are performed to reveal the cooperation relationship between different subunits. The conformational free energy analysis suggests that homo-tetramer subunits in not-standard D2-symmetry conformational pathways are more energetically advantageous compared to standard D2-symmetric pathways. In the sampled intermediate conformational states, some subunits show same subunit state, while others exhibit different subunit state, indicating that both coordinated and independent mechanism may exists during the catalytic process of four subunits.

Key subunit state affects ligand binding in the citryl-CoA synthesis process

The conformational changes of ACLY subunits have a significant coupling relationship with ligand binding and biochemical reactions in the experimental assays.[19,20] The intermediate-state cyro-EM structure of ACLY tetramer (PDB: 6uuw) has revealed the binding sites of

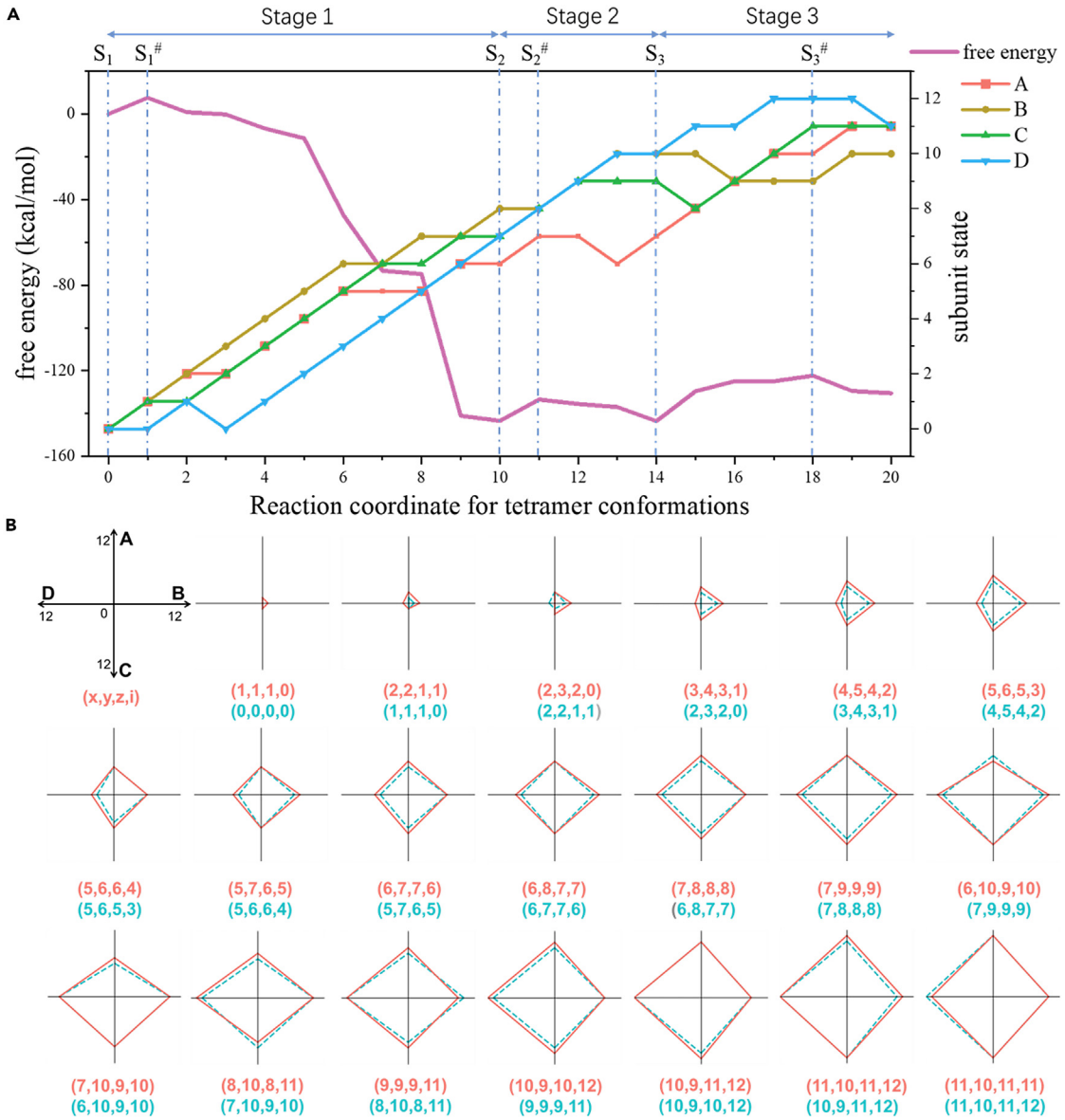

Figure 3. The key energetic and conformational changes along the optimal conformational pathway of ACLY tetramer during the citryl-CoA synthesis process

(A) The conformational free energy profile for ACLY tetramer is shown in solid gray. The entire process is divided into three stages based on the corresponding free energy barriers (i.e., from S_1 to $S_1^{\ddagger}$; from S_2 to $S_2^{\ddagger}$; from S_3 to $S_3^{\ddagger}$), which are marked by red dashed arrows. The conformational changes of subunit states are represented by colored lines for chains A, B, C, and D, respectively.

(B) The symmetries of four subunits for the tetramer conformations in the optimal pathway (shown in solid red) and their overlap with the tetramer conformations at last step (shown in dashed cyan) along the conformational coordinates of ACLY tetramer.

citryl-1-phosphate and CoA at the catalytic center of citryl-CoA synthesis,[21,23] which consists of eight residues including G281–283, S308, E599, G664–665, and S663 (see Figure 4A). Here, we analyzed the accessible tunnel for ligand binding to the catalytic center at different subunit states. The geometric parameters of citrate are used as the size of a molecular probe for tunnel detection, and detected tunnels are approximately modeled as a cylinder for volume calculation. Along the conformational pathway from subunit 0 to subunit 12, the radius of gyration of the catalytic center sharply decreases at subunit 1, and maintains relatively stable values until the end, suggesting that the catalytic center is probably formed at the state of subunit 1. Unlike the formation of the catalytic center, the tunnel volume accessible to the catalytic center decreases slowly from subunit 0 to subunit 6, and all the tunnels are closed after that (see Figure 4B). The accessibility of citrate probe to the catalytic center is constrained after the state of subunit 6 and completely blocked after the state of subunit 9, suggesting that the citrate is likely bounded before the state of subunit 6, and the related biochemical reactions happens with all the tunnels closed after subunit **9**.

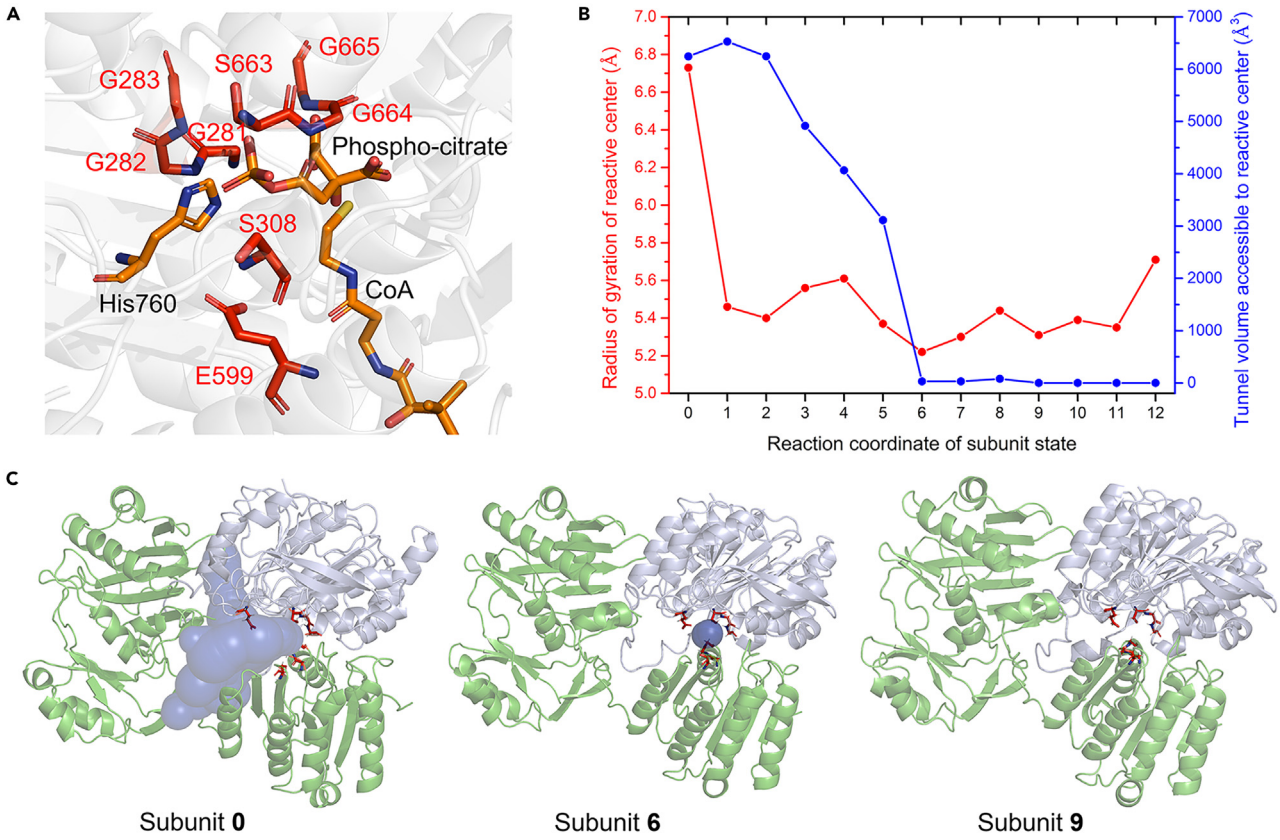

Figure 4. The properties of the catalytic center for conformational states of a single subunit from 0 to 12 during the citryl-CoA synthesis process

(A) the catalytic center, where key moieties interact to produce citryl-CoA (PDB: 6uuw). The key moieties involved in the synthesis of citryl-CoA including His760, phosphor-citrate, CoA are shown in orange sticks. Eight residues that define the catalytic center, G281–283, S308, E599, G664–665, and S663, are shown in red sticks.

(B) The changes in the radius of gyration of catalytic center (in red line) and the tunnel volume to the catalytic center (in blue line) during the citryl-CoA synthesis process.

(C) The presentation of the catalytic center and accessible tunnel for subunit 0, 6, and 9. The tunnels are shown as dark blue spheres. CCSβ and CCSα are represented in green and blue cartoons, respectively, while CCL domains are omitted.

In order to evaluate the influence of substrate binding on the free energy barriers along the conformational pathway, the binding free energies of substrates binding to intermediate conformations of ACLY monomer (from subunit 0 to subunit 12) were predicted through molecular modeling (see Videos S2, S3, and S4), as shown in Table S1. It can be seen that ligand binding could exhibit significant influence on the free energy changes in conformational pathway. Then, the influence of substrates binding to ACLY tetramer were calculated by adding up the binding energies of three substrates in different intermediate conformations of ACLY monomer, as shown in Table S2. Four molecules of ATP-Mg^{2+} binding from S(0,0,0,0) to S(1,1,1,0) might cause the free energy barrier change of +53.76 kcal/mol, while four molecules of citrate binding from S(6,8,7,7) to S(7,8,8,8) and CoA binding from S(7,10,9,10) to S(10,9,11,12) cause the free energy barrier change of +3.04 kcal/mol and +3.35 kcal/mol. The substrate binding may strengthen the conformational stability of the intermediate states and influence significantly on the conformational free energy barriers.

Key residues on ACLY affect the conformational free energy profile

Along the conformational free energy profile, a huge free energy change of less than −100 kcal/mol distinguished stage 1 from the other stages. The corresponding conformation states, S(4, 5, 4, 2) and S(6, 7, 7, 6), were further employed for electrostatic surface potential and per-residue energy contribution analysis. As shown in Figures S8 and S9, the electrostatic potential surface of the peripheral CCS domain and the central CCL domain exhibits a significant change in electrostatic distribution, primarily involving a series of charged residues including K166, K167, K178, K209, D210, K232, E249, D318, K554, K836, K964, E1009, and E1012. Furthermore, key residues involved in the activation barriers at different stages are also analyzed, as shown in Figure 5. The free energy barrier contributed by each residue was calculated and summed up to a single energy term (i.e., ΔΔG) for the same-numbering residues in four subunits. The stalk domain (sequence 810–838) is found to be crucial for the stability and symmetry of ACLY tetramer.[19] The breakdown of the hydrogen bonding between $D824^{A}$-$R829^{B}$,

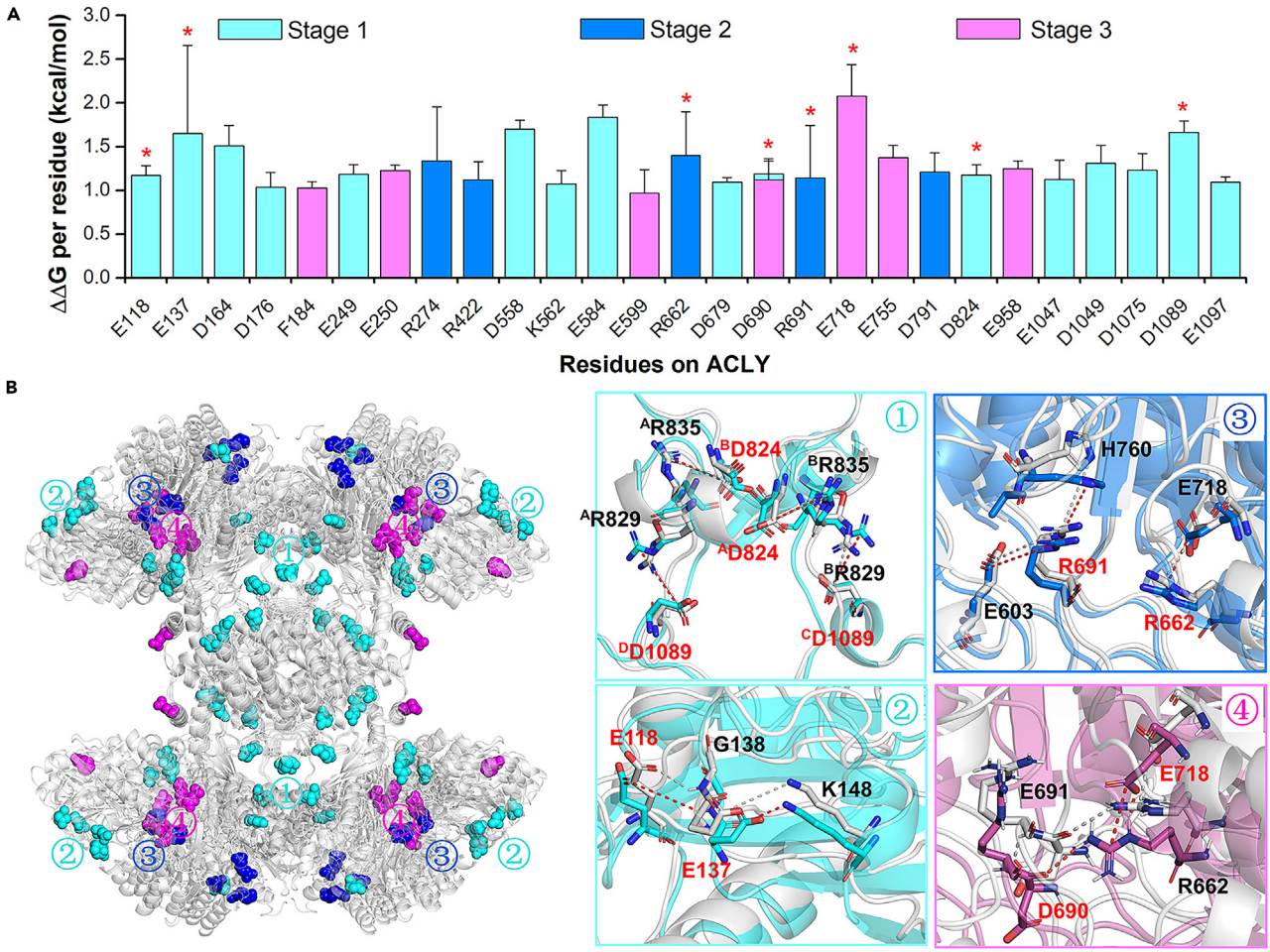

Figure 5. The per-residue contribution to the conformational free energy barriers during the citryl-CoA synthesis process

(A) the residues involved in the free energy barriers at stage 1–3 with per-residue contribution ($\Delta\Delta G$) higher than 1 kcal/mol. Residues labeled with red asterisks exhibit obvious changes in interactions associated with subunit interfaces or biochemical reactions. Data are represented as mean ± standard error of the mean (SEM), with standard error value as error bar.

(B) The distribution of recognized key residues on ACLY tetramer. The intermediate conformations (i.e., $S_1^{\ddagger}$, $S_2^{\ddagger}$, $S_3^{\ddagger}$) at stage 1–3 are aligned to the corresponding initial conformations (i.e., S_1, S_2, S_3) by C_α atoms for comparison. key residues recognized in intermediate conformations are depicted in cyan, blue and magenta cartoon/sphere/sticks respectively, and their involved interactions are shown in red dashed lines. The corresponding residues in the initial conformations are shown in gray, and the interactions are shown in gray dashed lines.

D824^{B}-R829^{A}, D835^{B}-R1089^{C}, and D835^{B}-R1089^{C} is observed during conformational change of stage 1. E118 is identified as an important residue for Mg^{2+}-ATP binding. Changes in the hydrogen bonding network are also observed among E118, E137, G138, and K148 for each subunit at stage 1. In stage 2, as the conformational change mainly acts as the pre-chemistry preparation for reaction (ii) and reaction (iii), key residues that affect the free energy barrier are mainly located adjacent to the reactive center including E603, R662, R691, H760, and E718, and they exhibit changes in the salt bridge network. The interaction network further affects this network in stage 3, highlighting the importance of R662, D690, R691, and E718 during the conformational change process.

Coupling between conformational change and biochemical reactions

The conformational analysis by small-angle X-ray scattering (SAXS) reveals that the conformational oscillation of ACLY tetramer is dependent on the ligand-binding manner,[19] which is also changeable with the reaction proceeding in the catalytic cycle. The sub-reactions associated with different substrates (Mg^{2+}-ATP, citrate, and CoA) happen in a specific order from reaction(i) to reaction(iii) during the citryl-CoA synthesis process.[14] We utilized the Michaelis constant (K_M) of each substrate, as well as the catalytic efficiency constant (k_{cat}/K_M), to represent the free energy changes and free energy barriers for three sub-reactions,[14] and the free energy profiles are presented in Figure S10. Furthermore, a three-dimensional potential surface is constructed by coupling the conformational free energies and chemical free energies together using a multi-minima treatment of the empirical valence bond approach.[39,45]

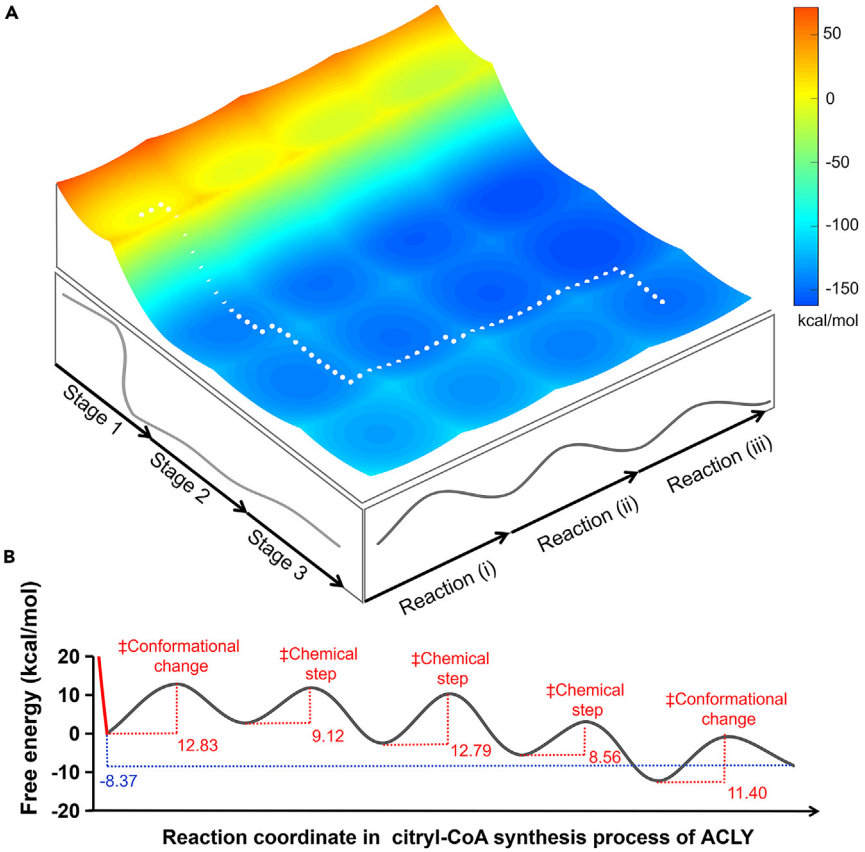

Figure 6. The energetic coupling between the conformational changes and biochemical reactions during the citryl-CoA synthesis process

(A) The complete free-energy surface for conformational changes (stage 1–3) and biochemical reactions (Reaction i to iii). Reaction (i): Mg^{2+}-ATP + E → E-P + Mg^{2+}-ADP; reaction (ii): E-P + Citrate → E.Citrate-P; reaction (iii): E.Citrate-P + CoA → E.Citryl-CoA + Pi; where E represents ACLY. The coupling pathway with the most possibilities with labeled out by white dashed lines.

(B) The free energy profile for reaction coordinate during the citryl-CoA synthesis process. The overall reaction is as follows: Mg^{2+}-ATP + Citrate + CoA → Citryl-CoA + Mg^{2+}-ADP + Pi. The coupled (solid) energy profile is depicted as follows: the red solid represents the significant free energy change in stage 1, while the gray solid represents the subsequent process. The main free energy barriers and the overall free energy change for the process are labeled.

As shown in Figure 6A, the coupled potential surface reveals the coupling relationship for three conformational stage and three biochemical reactions, providing fundamental insights into the kinetic features. The free energy landscape for the citryl-CoA synthesis process starts from the top-left state, where the ACLY tetramer is in an apo state; reaction (i) initially happens alongside the conformational changes in stage 1 and stage 2 and ends at the beginning of stage 3; subsequently, reaction (ii) and (iii) continuously happen in almost the same conformational state in stage 3; finally, the conformational change in stage 3 occurs after all the biochemical reactions. This is consistent with the kinetic researches that Mg^{2+}-ATP is first binding to activate ACLY tetramer and trigger the following biochemical reactions.[11] According to positional isotope exchange (PIX) studies,[14] the reaction (i) for ACLY is highly reversible and has the largest PIX rate (14 s^{-1}) reported so far, which suggests that the apo state is strongly driven to its phosphorylated state upon the binding of Mg^{2+}-ATP. The great tendency for the phosphorylation of ACLY is also in line with the low free energy barrier and significant free energy change in stage 1. Structural studies indicate that reaction (ii) and (iii) both happens at the catalytic center, constituted by G281–283, S308, E599, G664–665, and S663. According to the catalytic center and tunnel analysis in Figure 4, reaction (ii) and (iii) take place with all the tunnels closed after subunit 9, consistent with the results of energetic coupling showing that reaction (ii) and (iii) happen in stage 3.

The overall free energy profile for the citryl-CoA synthesis process is further presented in Figure 6B. The free energy changes and free energy barriers for each conformational stage and chemical reaction are coupled and differ from the original energy profiles, suggesting that conformational stages and chemical reactions are not separated events, but coupled with each other during the citryl-CoA synthesis process. The overall reaction for the synthesis of citryl-CoA is the sum of reaction (i)–(iii) as follows: Mg^{2+}-ATP + Citrate + CoA → Citryl-CoA + Mg^{2+}-ADP + Pi, and the free energy barrier for the rate-limiting step is estimated to be 12.83 kcal/mol. Our coupling free energy profile supports that the rate-limiting step occurs during the coupling process of stage 2 and reaction (i), possibly involving the product release of reaction (i) or the conformational change of phosphorylated ACLY for the following biochemical reactions. These predicted results are

comparable to the hypothesis that the desorption of Mg^{2+}-ADP is the rate-limiting step, with a rate of about 7 s^{-1} ($\Delta G^{\ddagger}$ = 16.29 kcal/mol), according to the kinetic model proposed by Fan et al.[14]

Conclusions

ACLY is an enzyme with a complex catalytic process. Its kinetic studies began in the 1960s, however, subsequent research has been seriously limited due to the lack of three-dimensional structures and efficient modeling techniques. Recent crystallographic and cyro-EM studies allow us to have a close look at the structural basis during the citryl-CoA synthesis process. We modeled the entire free energy landscape of tetramer conformations of ACLY to investigate the symmetrical mechanism among subunits and the potential coupling relationship between conformation changes and biochemical reactions. To determine the optimal conformational variation pathway, we constructed a free energy landscape comprising 13^4 modeled tetramer conformations and applied coarse-grained method for conformational free energy calculations. According to the optimal pathway determined through Monte Carlo method, the rigid D2 symmetry of ACLY tetramer is disrupted during the citryl-CoA synthesis process for the energetic advantage of conformational barriers and both coordinated and independent mechanism may exists during the catalytic process of four subunits. The energetic coupling between conformational changes and biochemical reactions suggests that these biological events are not independent but coupled with each other, and the coupled profile exhibits energy barrier values comparable to the experimental data at the rate-limiting step. Additionally, a series of interfacial residues between subunits has been predicted to significantly affect the conformational barriers. We believe that studies on conformations and energetics of ACLY subunits during the citryl-CoA synthesis process could provide insight into the mechanism research of the catalytic cycle of ACLY.

Limitations of the study

In order to speed up the pathway search, accelerated Monte Carlo algorithm was employed, which may result in a certain degree of loss in path sampling accuracy. The evaluation procedure for sampled pathways considered all emerging energy barriers. It's essential to note that pathway searching in high-dimensional space is a complex task, and guaranteeing the traversability of pathway sampling is challenging. Nevertheless, through a large number of samplings and evaluations, the sampled optimal pathway could be very close to the best pathways. Since kinetic studies on ACLY or its cognate proteins are seriously lacking, the predicted kinetic parameters for citryl-CoA synthesis process of ACLY were compared to the similar catalytic process between reactants and products. It is suggested that energetic coupling between conformational changes and biochemical reactions turn out to be an effective approach to reveal the relationship among these events.

STAR★METHODS

Detailed methods are provided in the online version of this paper and include the following:

- KEY RESOURCES TABLE
- RESOURCE AVAILABILITY
  - Lead contact
  - Materials availability
  - Data and code availability
- METHOD DETAILS
  - Building the initial tetramer systems
  - The energetics of the CG protein model
  - Construction of the free energy landscape of ACLY tetramer with arbitrary symmetry
  - Pathway search based on the entire free energy landscape of the ACLY tetramer
  - Energetic coupling of conformational change and biochemical reactions
  - Prediction of the properties of catalytic center and tunnels in subunit of ACLY
  - Prediction of key residues on ACLY based on the free energy barriers

SUPPLEMENTAL INFORMATION

Supplemental information can be found online at https://doi.org/10.1016/j.isci.2024.110605.

ACKNOWLEDGMENTS

This research was funded by the National Natural Science Foundation of Youth Fund Project, grant number 22103066; the 2021 Basic Research General Project of Shenzhen, China, grant number 20210316202830001; and the Warshel Institute for Computational Biology funding from Shenzhen City and Longgang District, grant number D10120180089.

AUTHOR CONTRIBUTIONS

Conceptualization, D.S. and C.B.; methodology, D.S. and X.Z.; validation, D.S.; formal analysis, D.S. and H.Z.; investigation, D.S. and J.Y.; resources, D.S. and C.B.; writing–original draft, D.S. and C.B.; writing–review & editing, D.S. and C.B.; visualization, D.S., H.Z., and J.Y.; supervision, C.B.; paoject administration, C.B.

DECLARATION OF INTERESTS

The authors declare no competing interests.

Received: October 30, 2023
Revised: June 3, 2024
Accepted: July 25, 2024
Published: July 27, 2024

REFERENCES

1. Khwairakpam, A.D., Banik, K., Girisa, S., Shabnam, B., Shakibaei, M., Fan, L., Arfuso, F., Monisha, J., Wang, H., Mao, X., et al. (2020). The vital role of ATP citrate lyase in chronic diseases. J. Mol. Med. *98*, 71–95. https://doi.org/10.1007/s00109-019-01863-0.
2. Pinkosky, S.L., Groot, P.H.E., Lalwani, N.D., and Steinberg, G.R. (2017). Targeting ATP-Citrate Lyase in Hyperlipidemia and Metabolic Disorders. Trends Mol. Med. *23*, 1047–1063. https://doi.org/10.1016/j.molmed.2017.09.001.
3. Zaidi, N., Swinnen, J.V., and Smans, K. (2012). ATP-citrate lyase: a key player in cancer metabolism. Cancer Res. *72*, 3709–3714. https://doi.org/10.1158/0008-5472.CAN-11-4112.
4. Chypre, M., Zaidi, N., and Smans, K. (2012). ATP-citrate lyase: a mini-review. Biochem. Biophys. Res. Commun. *422*, 1–4. https://doi.org/10.1016/j.bbrc.2012.04.144.
5. Grevengoed, T.J., Klett, E.L., and Coleman, R.A. (2014). Acyl-CoA metabolism and partitioning. Annu. Rev. Nutr. *34*, 1–30. https://doi.org/10.1146/annurev-nutr-071813-105541.
6. Puccini, J., Wei, J., Tong, L., and Bar-Sagi, D. (2023). Cytoskeletal association of ATP citrate lyase controls the mechanodynamics of macropinocytosis. Proc. Natl. Acad. Sci. USA *120*, e2213272120. https://doi.org/10.1073/pnas.2213272120.
7. Wellen, K.E., Hatzivassiliou, G., Sachdeva, U.M., Bui, T.V., Cross, J.R., and Thompson, C.B. (2009). ATP-citrate lyase links cellular metabolism to histone acetylation. Science *324*, 1076–1080. https://doi.org/10.1126/science.1164097.
8. Granchi, C. (2018). ATP citrate lyase (ACLY) inhibitors: An anti-cancer strategy at the crossroads of glucose and lipid metabolism. Eur. J. Med. Chem. *157*, 1276–1291. https://doi.org/10.1016/j.ejmech.2018.09.001.
9. Migita, T., Okabe, S., Ikeda, K., Igarashi, S., Sugawara, S., Tomida, A., Soga, T., Taguchi, R., and Seimiya, H. (2014). Inhibition of ATP citrate lyase induces triglyceride accumulation with altered fatty acid composition in cancer cells. Int. J. Cancer *135*, 37–47. https://doi.org/10.1002/ijc.28652.
10. Inoue, H., Tsunemi, T., Suzuki, F., and Takeda, Y. (1969). Studies on ATP citrate lyase of rat liver. IV. The role of CoA. J. Biochem. *65*, 889–900. https://doi.org/10.1093/oxfordjournals.jbchem.a129093.
11. Plowman, D.M., and Cleland, W.W. (1967). Purification and kinetic studies of the citrate cleavage enzyme. J. Biol. Chem. *242*, 4239–4247.
12. Srere, P.A., and Bhaduri, A. (1964). The Citrate Cleavage Enzyme. Iii. Citryl Coenzyme a as a Substrate and the Stereospecificity of the Enzyme. J. Biol. Chem. *239*, 714–718.
13. Walsh, C.T., Jr., and Spector, L.B. (1969). Citryl phosphate and the mode of action of the citrate cleavage enzyme. J. Biol. Chem. *244*, 4366–4374.
14. Fan, F., Williams, H.J., Boyer, J.G., Graham, T.L., Zhao, H., Lehr, R., Qi, H., Schwartz, B., Raushel, F.M., and Meek, T.D. (2012). On the catalytic mechanism of human ATP citrate lyase. Biochemistry *51*, 5198–5211. https://doi.org/10.1021/bi300611s.
15. Aoshima, M., Ishii, M., and Igarashi, Y. (2004). A novel enzyme, citryl-CoA synthetase, catalysing the first step of the citrate cleavage reaction in Hydrogenobacter thermophilus TK-6. Mol. Microbiol. *52*, 751–761. https://doi.org/10.1111/j.1365-2958.2004.04009.x.
16. Srere, P.A. (1963). Citryl-CoA. An substrate for the citrate-cleavage enzyme. Biochim. Biophys. Acta *73*, 523–525.
17. Verstraete, K., Verschueren, K.H.G., Dansercoer, A., and Savvides, S.N. (2021). Acetyl-CoA is produced by the citrate synthase homology module of ATP-citrate lyase. Nat. Struct. Mol. Biol. *28*, 636–638. https://doi.org/10.1038/s41594-021-00624-3.
18. Aoshima, M., Ishii, M., and Igarashi, Y. (2004). A novel enzyme, citryl-CoA lyase, catalysing the second step of the citrate cleavage reaction in Hydrogenobacter thermophilus TK-6. Mol. Microbiol. *52*, 763–770. https://doi.org/10.1111/j.1365-2958.2004.04010.x.
19. Verschueren, K.H.G., Blanchet, C., Felix, J., Dansercoer, A., De Vos, D., Bloch, Y., Van Beeumen, J., Svergun, D., Gutsche, I., Savvides, S.N., and Verstraete, K. (2019). Structure of ATP citrate lyase and the origin of citrate synthase in the Krebs cycle. Nature *568*, 571–575. https://doi.org/10.1038/s41586-019-1095-5.
20. Wei, J., Leit, S., Kuai, J., Therrien, E., Rafi, S., Harwood, H.J., Jr., DeLaBarre, B., and Tong, L. (2019). An allosteric mechanism for potent inhibition of human ATP-citrate lyase. Nature *568*, 566–570. https://doi.org/10.1038/s41586-019-1094-6.
21. Wei, X., Schultz, K., Bazilevsky, G.A., Vogt, A., and Marmorstein, R. (2020). Molecular basis for acetyl-CoA production by ATP-citrate lyase. Nat. Struct. Mol. Biol. *27*, 33–41. https://doi.org/10.1038/s41594-019-0351-6.
22. Wei, X., Schultz, K., Pepper, H.L., Megill, E., Vogt, A., Snyder, N.W., and Marmorstein, R. (2023). Allosteric role of the citrate synthase homology domain of ATP citrate lyase. Nat. Commun. *14*, 2247. https://doi.org/10.1038/s41467-023-37986-9.
23. Wei, X., and Marmorstein, R. (2021). Reply to: Acetyl-CoA is produced by the citrate synthase homology module of ATP-citrate lyase. Nat. Struct. Mol. Biol. *28*, 639–641. https://doi.org/10.1038/s41594-021-00625-2.
24. Bazilevsky, G.A., Affronti, H.C., Wei, X., Campbell, S.L., Wellen, K.E., and Marmorstein, R. (2019). ATP-citrate lyase multimerization is required for coenzyme-A substrate binding and catalysis. J. Biol. Chem. *294*, 7259–7268. https://doi.org/10.1074/jbc.RA118.006685.
25. Bennett, M.J., Schlunegger, M.P., and Eisenberg, D. (1995). 3D domain swapping: a mechanism for oligomer assembly. Protein Sci. *4*, 2455–2468. https://doi.org/10.1002/pro.5560041202.
26. Andre, I., Strauss, C.E., Kaplan, D.B., Bradley, P., and Baker, D. (2008). Emergence of symmetry in homooligomeric biological assemblies. Proc. Natl. Acad. Sci. USA *105*, 16148–16152. https://doi.org/10.1073/pnas.0807576105.
27. Wolynes, P.G. (1996). Symmetry and the energy landscapes of biomolecules. Proc. Natl. Acad. Sci. USA *93*, 14249–14255. https://doi.org/10.1073/pnas.93.25.14249.
28. Goodsell, D.S., and Olson, A.J. (2000). Structural symmetry and protein function. Annu. Rev. Biophys. Biomol. Struct. *29*, 105–153. https://doi.org/10.1146/annurev.biophys.29.1.105.
29. Brennecke, J.T., and de Groot, B.L. (2018). Quantifying Asymmetry of Multimeric Proteins. J. Phys. Chem. A *122*, 7924–7930. https://doi.org/10.1021/acs.jpca.8b06843.
30. Schopf, P., and Warshel, A. (2014). Validating Computer Simulations of Enantioselective Catalysis; Reproducing the Large Steric and Entropic Contributions in Candida Antarctica Lipase B. Proteins *82*, 1387–1399. https://doi.org/10.1002/prot.24506.
31. Vorobyov, I., Kim, I., Chu, Z.T., and Warshel, A. (2016). Refining the treatment of membrane proteins by coarse-grained models. Proteins *84*, 92–117. https://doi.org/10.1002/prot.24958.
32. Vicatos, S., Rychkova, A., Mukherjee, S., and Warshel, A. (2014). An Effective Coarse-Grained Model for Biological Simulations: Recent Refinements and Validations. Proteins *82*, 1168–1185. https://doi.org/10.1002/prot.24482.
33. Metropolis, N., Rosenbluth, A.W., Rosenbluth, M.N., Teller, A.H., and Teller, E. (1953). Equation of state calculations by fast computing machines. J. Chem. Phys. *21*, 1087–1092.
34. Warshel, A., Sharma, P.K., Kato, M., and Parson, W.W. (2006). Modeling electrostatic effects in proteins. Biochim. Biophys. Acta *1764*, 1647–1676. https://doi.org/10.1016/j.bbapap.2006.08.007.
35. Mukherjee, S., Bora, R.P., and Warshel, A. (2015). Torque, chemistry and efficiency in molecular motors: a study of the rotary-chemical coupling in F1-ATPase. Q. Rev. Biophys. *48*, 395–403. https://doi.org/10.1017/S0033583515000050.
36. Mukherjee, S., and Warshel, A. (2015). Brønsted slopes based on single-molecule imaging data help to unveil the chemically coupled rotation in F1-ATPase. Proc. Natl.

Acad. Sci. USA *112*, 14121–14122. https://doi.org/10.1073/pnas.1519066112.

37. Mukherjee, S., and Warshel, A. (2015). Dissecting the role of the γ-subunit in the rotary-chemical coupling and torque generation of F1-ATPase. Proc. Natl. Acad. Sci. USA *112*, 2746–2751. https://doi.org/10.1073/pnas.1500979112.
38. Bai, C., and Warshel, A. (2019). Revisiting the protonmotive vectorial motion of F0-ATPase. Proc. Natl. Acad. Sci. USA *116*, 19484–19489. https://doi.org/10.1073/pnas.1909032116.
39. Bai, C., Asadi, M., and Warshel, A. (2020). The catalytic dwell in ATPases is not crucial for movement against applied torque. Nat. Chem. *12*, 1187–1192. https://doi.org/10.1038/s41557-020-0549-6.
40. Rychkova, A., Mukherjee, S., Bora, R.P., and Warshel, A. (2013). Simulating the Pulling of Stalled Elongated Peptide from the Ribosome by the Translocon. Proc. Natl. Acad. Sci. USA *110*, 10195–10200. https://doi.org/10.1073/pnas.1307869110.
41. Adamczyk, A.J., and Warshel, A. (2011). Converting Structural Information into an Allosteric-Energy-Based Picture for Elongation Factor Tu Activation by the Ribosome. Proc. Natl. Acad. Sci. USA *108*, 9827–9832. https://doi.org/10.1073/pnas.1105714108.
42. Alhadeff, R., and Warshel, A. (2020). A free-energy landscape for the glucagon-like peptide 1 receptor GLP1R. Proteins *88*, 127–134. https://doi.org/10.1002/prot.25777.
43. Bai, C., Wang, J., Mondal, D., Du, Y., Ye, R.D., and Warshel, A. (2021). Exploring the activation process of the β2AR-Gs complex. J. Am. Chem. Soc. *143*, 11044–11051. https://doi.org/10.1021/jacs.1c03696.
44. Shi, D., An, K., Zhang, H., Xu, P., and Bai, C. (2022). Application of Coarse-Grained (CG) Models to Explore Conformational Pathway of Large-Scale Protein Machines. Entropy *24*, 620. https://doi.org/10.3390/e24050620.
45. Mukherjee, S., and Warshel, A. (2011). Electrostatic Origin of the Mechanochemical Rotary Mechanism and the Catalytic Dwell of F1-Atpase. Proc. Natl. Acad. Sci. USA *108*, 20550–20555. https://doi.org/10.1073/pnas.1117024108.
46. Le Guilloux, V., Schmidtke, P., and Tuffery, P. (2009). Fpocket: an open source platform for ligand pocket detection. BMC Bioinf. *10*, 168–178. https://doi.org/10.1186/1471-2105-10-168.
47. Frisch, M.J., Trucks, G.W., Schlegel, H.B., Scuseria, G.E., Robb, M.A., Cheeseman, J.R., Scalmani, G., Barone, V., Petersson, G.A., Nakatsuji, H., et al. (2009). Gaussian 09. https://gaussian.com/glossary/g09/.
48. Hamelberg, D., Mongan, J., and McCammon, J.A. (2004). Accelerated molecular dynamics: a promising and efficient simulation method for biomolecules. J. Chem. Phys. *120*, 11919–11929. https://doi.org/10.1063/1.1755656.
49. Kuczera, G., and Parent, E. (1998). Monte Carlo assessment of parameter uncertainty in conceptual catchment models: the Metropolis algorithm. J. Hydrol. X. *211*, 69–85. https://doi.org/10.1016/S0022-1694(98)00198-X.
50. Lobanov, M.Y., Bogatyreva, N.S., and Galzitskaya, O.V. (2008). Radius of gyration as an indicator of protein structure compactness. Mol. Biol. *42*, 623–628. https://doi.org/10.1134/S0026893308040195.
51. Hu, J., Komakula, A., and Fraser, M.E. (2017). Binding of hydroxycitrate to human ATP-citrate lyase. Acta Crystallogr. D *73*, 660–671. https://doi.org/10.1107/S2059798317009871.
52. Sun, T., Hayakawa, K., and Fraser, M.E. (2011). ADP-Mg2+ bound to the ATP-grasp domain of ATP-citrate lyase. Acta Crystallogr. F *67*, 1168–1172. https://doi.org/10.1107/S1744309111028363.
53. Wei, X., and Marmorstein, R. (2021). Reply to: Acetyl-CoA is produced by the citrate synthase homology module of ATP-citrate lyase. Nat. Struct. Mol. Biol. *28*, 639–641. https://doi.org/10.1038/s41594-021-00625-2.
54. Sun, T., Hayakawa, K., Bateman, K.S., and Fraser, M.E. (2010). Identification of the Citrate-binding Site of Human ATP-Citrate Lyase Using X-ray Crystallography. J. Biol. Chem. *285*, 27418–27428. https://doi.org/10.1074/jbc.M109.078667.
55. Trott, O., and Olson, A.J. (2010). AutoDock Vina: Improving the speed and accuracy of docking with a new scoring function, efficient optimization, and multithreading. J. Comput. Chem. *31*, 455–461. https://doi.org/10.1002/jcc.21334.
56. El Malki, Z., Bouzzine, S.M., Bejjit, L., Haddad, M., Hamidi, M., and Bouachrine, M. (2011). Density functional theory [B3LYP/6-311G(d,p)] study of a new copolymer based on carbazole and (3,4-Ethylenedioxythiophene) in their aromatic and polaronic states. J. Appl. Polym. Sci. *122*, 3351–3360. https://doi.org/10.1002/app.34395.
57. Dryga, A., and Warshel, A. (2012). Coarse Grained Model for Exploring Voltage Dependent Ion Channels. Biophys. J. *102*, 686a. https://doi.org/10.1016/j.bpj.2011.11.3730.

STAR★METHODS

KEY RESOURCES TABLE

REAGENT or RESOURCE	SOURCE	IDENTIFIER
Deposited data		
AMBER parameter database	Bryce group, University of Manchester	http://amber.manchester.ac.uk/
Software and algorithms		
Molaris-XG software	Vicatos et al.[32]	https://laetro.usc.edu/molaris.html
VMD version 1.9.3	Visual Molecular Dynamics, University of Illinois	https://www.ks.uiuc.edu/Research/vmd/
fpocket software	Le Guilloux et al.[46]	https://fpocket.sourceforge.net/
AutoDock Vina 1.1.2	The Scripps Research Institute, CCSB	https://vina.scripps.edu/
Gaussian09	Frisch et al.[47]	https://gaussian.com/glossary/g09/
PyMOL(TM) 2.5.4	Schrodinger, LLC	https://pymol.org/
Python version 3.7	Python Software Foundation	https://www.python.org

RESOURCE AVAILABILITY

Lead contact

Further information and requests for resources and reagents should be directed to and will be fulfilled by the Lead Contact, Dr Chen Bai (baichen@cuhk.edu.cn).

Materials availability

This study did not generate new unique reagent.

Data and code availability

- Data reported in this paper will be shared by the lead contact upon request.
- This paper does not report original code.
- Any additional information required to reanalyze the data reported in this paper is available from the lead contact upon request.

METHOD DETAILS

Building the initial tetramer systems

In this study, we used cryo-EM structures (PDB: 6pof, 6uuw) to model the conformational transition of ACLY tetramer from the apo state to the intermediate state during the citryl-CoA synthesis process.[21] In both structures, the three-dimensional coordinates for the amino acid sequence 2–425, 487–1099 in four subunits were retained for model construction. It's indicated that the catalytic process for ACLY tetramer could proceed as normal even with the structural deficiency of the loop sequence 426–486 *in vitro*.[19] Therefore, both systems were built with the loop sequence 426–486 missing, while further structural completion were performed for other structural absences. For system of 6pof, the loop sequence 751–766 were completed, referring to the corresponding coordinates in the chain B of another crystal structure[19] (PDB: 6qfb) with the alignment of Cα atoms adjacent to the loop sequence 751–766 in each subunit. For system of 6uuw, the loop sequence 140–148 were completed, referring to the corresponding coordinates in the chain B of the structure (PDB: 6qfb) with the alignment of Cα atoms adjacent to the loop sequence 140–148 in each subunit. All ligands in the structure (PDB: 6uuw) were deleted, for the atomic consistency in both structures. In the following modeling procedure, both the tetramers and the single subunit in each tetramer were applied in the conformational energy calculation.

The energetics of the CG protein model

The CG models have been widely applied for the conformational and energetic studies, especially for those enormous biological systems comprised of thousands of residues. In this study, we used an effective CG model developed by Warshel and coworkers to calculate the energetics of the CG protein model in Molaris-XG software package.[32] Based on a solvation model of ionizable residues, the CG model

achieved better performance in electrostatics free-energy evaluation than other CG models by emphasizing the crucial role of electrostatic effects in proteins.[34] In the CG model, the total CG free energy is given by:

$$\Delta G_{fold} = \Delta G_{main} + \Delta G_{side} + \Delta G_{main/side} \quad \text{(Equation 1)}$$

$$\Delta G_{main} = c_2 \Delta G^{CG}_{solv} + c_3 \Delta G^{CG}_{HB} \quad \text{(Equation 2)}$$

$$\Delta G_{side} = \Delta G^{elec}_{side} + \Delta G^{polar}_{side} + \Delta G^{hyd}_{side} + c_1 \Delta G^{vdw}_{side} \quad \text{(Equation 3)}$$

$$\Delta G_{main/side} = \Delta G^{elec}_{main/side} + \Delta G^{vdw}_{main/side} \quad \text{(Equation 4)}$$

The total CG folding free energy accounts for three terms, namely the main chain, side chain, and the total protein and side chain flexibility in estimating the overall conformational entropy as in *formula* (1). In detail, the main chain term ΔG_{main} constitutes two parts, i.e., the contribution from the backbones solvation and the hydrogen bonds (HB) as in *formula* (2); the side chain term ΔG_{side} is given by the electrostatic, polar, hydrophobic components and the van der Waals component for side chain interactions as in *formula* (3); The main chain/side chain coupling term consists of two parts, the electrostatic and the van der Waals parts as in *formula* (4). The detailed terms ΔG^{vdw}_{side}, ΔG^{CG}_{solv}, ΔG^{CG}_{HB}, ΔG^{elec}_{side}, ΔG^{polar}_{side}, ΔG^{hyd}_{side}, $\Delta G^{elec}_{main/side}$ and $\Delta G^{vdw}_{main/side}$ represent the sidechain van der Waals interaction, the mainchain solvation energy, the mainchain hydrogen bond force, the sidechain electrostatic effect, polar, hydrophobic contribution, main chain/side chain electrostatic energy, the mainchain/sidechain van der Waals interaction, respectively. Scaling coefficients c_1, c_2 and c_3 have values of 0.10, 0.25 and 0.15, respectively in this formula.

The focus is placed on the electrostatic term including ΔG^{elec}_{side} and $\Delta G^{elec}_{main/side}$. ΔG^{elec}_{side} is computed as a sum of change in free energy associated with charge-charge interactions between ionizable side chains $\Delta\Delta G^{w\rightarrow p}_{QQ}$, and the change in solvation free energy of those residues in their specific environment, $\Delta\Delta G^{w\rightarrow p}_{self}$, inside the protein and in water as in *formula* (5). While $\Delta G^{elec}_{main/side}$ is treated with the same electrostatic interaction form as in side chain electrostatic term but with a different $\boldsymbol{\varepsilon}$*eff*.

$$\Delta G^{elec}_{side} = \Delta\Delta G^{w\rightarrow p}_{QQ} + \Delta\Delta G^{w\rightarrow p}_{self} \quad \text{(Equation 5)}$$

Finally, if electrodes and electrolytes are presented, then another term is added to the total energy:

$$\Delta G = \Delta G^{CG}_{fold} + \Delta G^{CG}_{lyte-voltage}(V_{ext}) \quad \text{(Equation 6)}$$

Before the CG energy evaluation, we performed energy minimization and relaxation runs on each structure until the energy is converged, then applied a Monte Carlo Proton Transfer (MCPT) algorithm[31] to obtain the charge configuration of the system. In the MCPT approach, the MC controls proton transfer between ionizable residues or between one ionizable residue and the bulk. The acceptance possibility of the move is determined by standard Metropolis criteria.[33] The actual MCPT can be used for time dependent study of proton transport processes as described. However, here we use this approach just to obtained equilibrated ionization states. All CG free energy calculations were performed using the Molaris-XG software package.

Construction of the free energy landscape of ACLY tetramer with arbitrary symmetry

Due to the D2 symmetry of solved tetramer structures, the conformational change of each monomer was firstly explored and its free energy profile could be depicted. To investigate how the ACLY monomer is transformed from the initial apo state to the intermediate state, we generated the free energy profile using the representative ACLY monomer of each state.

Initially, the conformational energies for the subunits in the apo state and the intermediate state were calculated by the method described in the above section. In both states, the subunit showing the median folding energy values among four subunits was picked up for the following modeling. As shown in Figure S1, the subunit of chain C for the apo state and the subunit of chain B for the intermediate state were selected. Subsequently, we performed targeted molecular dynamics (TMD) to generate the intermediate conformations between the apo and intermediate states in Molaris-XG software package. In order to differentiate the conformations of single subunits, the apo-state and intermediate-state subunit conformations were numbered as subunit **0** and subunit **12**, and the generated 11 intermediate conformations were numbered as subunit **1**–**11**. Therefore, a total of 13 subunit states were applied to construct the conformations of the ACLY tetramer with arbitrary symmetry.

The subunit states **0**–**12** were recombined in the homo-tetrameric state of ACLY, and the recombined tetramer conformations were depicted by four numbers, for example the apo-state tetramer and the intermediate-state tetramer were named as **S** (**0**,**0**,**0**,**0**) and **S** (**12**,**12**,**12**,**12**) respectively. It's suggested that CCL domains (sequence 838–1099) of subunits closely assemble with D2 symmetry at the center of ACLY in homo-tetrameric state despite of the diverse symmetries of subunits.[19] Considering that, subunits on the recombined tetramer conformations were built by aligning the Cα atoms of CCL domain relative to the initial tetramer state in the VMD software (version 1.9.3). In that way, the entire conformational space containing a total of 134 tetramer conformations were constructed, and can be depicted as **S** (**x**, **y**, **z**, **i**) with **x**, **y**, **z**, **i** ranging from **0** to **12**. The conformational energies were then calculated by the method described in the above section.

Pathway search based on the entire free energy landscape of the ACLY tetramer

Based on the construction of the conformations and energetics of ACLY tetramer, a free energy landscape for the conformational change of ACLY tetramer was built and the optimal conformational change pathway was sampled using the Monte Carlo sampling method as shown in the workflow chart in Figure S2. The main process is divided into three sections as follows.

(1) The scaling process is performed to reconstruct the free energy landscape by accelerated molecular dynamics simulation (AMD) method[48] in blue section of Figure S2. In detail, the new free energy value (E_s') for the conformations of ACLY tetramer was scaled based on the original free energy value (E_s) as follows:

$$E_s' = E_s + \frac{[E_s(max) - E_s]^2}{k[E_s(max) - E_s(min)] + [E_s(max) - E_s]} \quad \text{(Equation 7)}$$

Where $E_s(max)$, $E_s(min)$ represent the maximum and minimum energy values in the original free energy landscap, while k is a scaling factor with value of 0.1.

(2) The sampling process is performed to search possible pathways via the Metropolis sampling process[49] in red section of Figure S2. The conformational pathway starts at **S (0,0,0,0)** and ends at **S (12,12,12,12)**. The move of conformational state for each subunit can be set as, meaning one step forward, staying, and one step backward respectively. The possibilities for the move of one subunit satisfies *formula* (8) as follows:

$$P_{-1} + P_0 + P_{+1} = 1 \quad \text{(Equation 8)}$$

In this study, (P_{-1}, P_0, P_{+1}) are set with values of (0.1, 0.45, 0.45), (0.2, 0.4, 0.4) and (0.3, 0.35, 0.35) and applied for pathway sampling respectively. The entire move of conformational state for tetramer can further be depicted as m (i,j,l,k),i,j,l,k $\in$ [+1,0, − 1], and the possibility for the move of four subunits can be calculated as follows:

$$P_m = P_i * P_j * P_l * P_m \quad \text{(Equation 9)}$$

Each move selection was made randomly based on its relative possibility among all potential move ensemble by normalization. Then, a new conformational state of tetramer can be achieved after the move selection. The acceptance of the new conformational state is based on its free energy barriers according to the Monte Carlo method as follows:

$$random(0,1) \leq e^{-\frac{\Delta E}{k_b T}} \quad \text{(Equation 10)}$$

(3) The scoring process is conducted to evaluate the sampled pathways the Arrhenius equation and scoring function in green block of Figure S2. 10000 conformational pathways are sampled by the Metropolis sampling process. For all the sampled conformational pathways, the redundant conformations that occurring more than twice were firstly deleted from the original pathway. The truncated pathway with no redundant conformations was further applied for average free energy barrier calculation by considering all the occurred free energy barriers along the pathway. Firstly, the rate constant for each barrier was calculated referring to the Arrhenius equation as shown in Equation 11. Then, the average rate constant was calculated as shown in Equation 12, and set as a criterion for the selection of the optimal pathways.

$$k_i \propto e^{-\frac{\Delta E_i^{\ddagger}}{RT}} \quad \text{(Equation 11)}$$

$$\text{score} = \frac{1}{\sum_{i=1}^{N} \frac{1}{k_i}} \quad \text{(Equation 12)}$$

Finally, we obtained the conformational and energetic profiles for the conformational change of ACLY tetramer during the citryl-CoA synthesis process. The pathway search workflow using the Monte Carlo sampling method were implemented via scripting in Python.

Energetic coupling of conformational change and biochemical reactions

During the citryl-CoA synthesis process, the total energy of the system can be defined as follows:

$$E_{tot} = E^{conf} + E^{bind/chem} \quad \text{(Equation 13)}$$

Where the free energy change of E^{conf} can be obtained through the calculation of the conformational energies above, while the free energy change of $E^{bind/chem}$ are obtained through the prediction based on experimental data.

In order to effectively obtain the potential energy surface of the conformational change in the citryl-CoA synthesis process, we construct a Hamiltonian whose diagonal states represent the key minimal states before and after the conformational change occurs. The effective potential energy surface of the conformational energy can be obtained by diagonalizing the Hamiltonian matrix:

$$H_g^{conf} C_g = E_g^{conf} C_g \quad \text{(Equation 14)}$$

The diagonal elements of the Hamiltonian matrix can be described by the following equation:

$$H_{ll}^{conf} = \frac{1}{2}\hbar\omega_Q \left(Q - \delta_Q^l\right)^2 + \alpha_l \quad \text{(Equation 15)}$$

where $\hbar$ is the reduced Planck constant, ω_Q represents the effective vibrational frequency of the corresponding state, $\hbar\omega_Q$ has units of energy, Q is the dimensionless reaction coordinate modeling the system, δ_Q^l is the positional offset of the minimum point along the reaction coordinate, and α_l represents the energy difference between the diagonal energy minima. The index l can take on values 1, 2, 3 … up to the total number of intermediate states, and ll corresponds to the diagonal elements of H_g^{conf}.

To reproduce the free energy change and barrier height of the conformational change process, we fit the non-diagonal elements of H_g^{conf} and the numerical values of δ_Q^l. Similarly, for the Hamiltonian $H_g^{bind/chem}$ describing substrate binding and chemical reaction, we apply a similar approach as H_g^{conf}. Furthermore, we applied a Monte Carlo sampling method to construct the coupling between all occurring events using the obtained reduced free energy surfaces. A necessary condition for the Monte Carlo sampling order on the free energy surface is also derived as Equation 10. The energetic coupling using the Monte Carlo sampling method were implemented via scripting in Python.

Prediction of the properties of catalytic center and tunnels in subunit of ACLY

The catalytic center of each subunit of ACLY is defined by eight residues including G281–283, S308, E599, G664–665, S663. The radius of gyration[50] of catalytic center is calculated for subunit states **0**–**12**. The volume of the tunnels that have access to the catalytic center was further calculated for all subunit states in the fpocket software.[46] The probe_radius is defined as 2.5 Å referring to molecular size of citrate, while other parameters were set as default. The bottleneck radius (r_i) and Length (L_i) for all the accessible tunnel can be achieved through the prediction. Then, the overall volumes (V) were estimated by taking the tunnels as cylinder as follows:

$$V = \sum_{i=1}^{N} \pi r_i^2 L_i \quad \text{(Equation 16)}$$

Prediction of the binding free energies of substrates (ATP-Mg2+, Citrate, CoA) binding to the active sites of intermediate states for ACLY.

The initial binding poses of substrates (ATP-Mg2+, Citrate, CoA) binding to their active sites were generated from the prediction of molecular docking for each intermediate structures. The active sites for three substrates were defined by the key residues reported in the crystal or cyro-EM structures, namely residues (residue numbers 8, 56, 58, 63–68, 72, 74, 108–111, 113, 115, 118, 139–140, 203–204, 215–216) for ADP binding in crystal or cyro-EM structures (PDB: 5tdm,[51] 3pff,[52] 7liw [53]), residues (residue numbers 280–281, 307–310, 343–348, 379, 626, 664–665) for citrate binding in crystal structures (PDB:3mwd,[54] 5tde [51]), residues (residue numbers 261, 309, 347, 505, 533, 572–574, 576–577, 597–599, 624–626, 664–665, 964, 969–970, 973–974, 1014, 1017–1018, 1021) for CoA binding in cyro-EM structures (PDB: 7liw). The monomer intermediate structures, namely subunit **0** to subunit **12**, were used as receptor for ATP-Mg2+ and citrate binding, while the tetramer intermediate structures with same subunit states, namely S(**0**,**0**,**0**,**0**) to S(**12**,**12**,**12**,**12**), were used as receptor for CoA binding. Three substrates were docked into ACLY by a sophisticated gradient optimization method in the AutoDock Vina software.[55] For each complex state of substrate and receptor, the top 10 binding poses were analyzed to find the best ligand–protein binding mode based on the scoring function. In order to calculate the binding free energy, the partial atomic charges of citrate and CoA were obtained by the electrostatic potential (esp) calculation with hybrid density functional theory (DFT) at the level of b3lyp/6-311g (d,p) in Gaussian09 software,[47,56] while the partial atomic charges of ATP was derived from the AMBER parameter database (http://amber.manchester.ac.uk/). Then, certain characteristics of three substrates were incorporated into the Molaris-XG force field, including the names, types and charges of atoms and bond information. PDLD/S-LRA/ method is used to calculate the binding free energy between each substrate and its receptor by all-atom structures.[57] The Molaris-XG software package was utilized for all relative calculations.

Prediction of key residues on ACLY based on the free energy barriers

The key residues that have significant contribution to the free energy barriers during the conformational change of ACLY tetramer were further recognized. In order to analyze the contribution for free energy barrier, the residue-specific energy decomposition was conducted for the

starting state ($E_{start}^{residue}$) and transition state ($E_{transition}^{residue}$) of the conformational barrier from the CG free energy calculations in Molaris-XG software package. The contribution of each residue ($\Delta G_{residue}$) is calculated as follows:

$$\Delta G_{residue} = E_{transition}^{residue} - E_{start}^{residue} \quad \text{(Equation 17)}$$

All the representations of electrostatic surfaces, key residues and substrate-binding poses of ACLY subunit or tetramer in this study are depicted in the PyMOL(TM) 2.5.4 software.